

Faraday Discussions

Accepted Manuscript



This manuscript will be presented and discussed at a forthcoming Faraday Discussion meeting. All delegates can contribute to the discussion which will be included in the final volume.

Register now to attend! Full details of all upcoming meetings: <http://rsc.li/fd-upcoming-meetings>



This is an *Accepted Manuscript*, which has been through the Royal Society of Chemistry peer review process and has been accepted for publication.

Accepted Manuscripts are published online shortly after acceptance, before technical editing, formatting and proof reading. Using this free service, authors can make their results available to the community, in citable form, before we publish the edited article. We will replace this *Accepted Manuscript* with the edited and formatted *Advance Article* as soon as it is available.

You can find more information about *Accepted Manuscripts* in the [Information for Authors](#).

Please note that technical editing may introduce minor changes to the text and/or graphics, which may alter content. The journal's standard [Terms & Conditions](#) and the [Ethical guidelines](#) still apply. In no event shall the Royal Society of Chemistry be held responsible for any errors or omissions in this *Accepted Manuscript* or any consequences arising from the use of any information it contains.

Structure-charge relationship – the case of hematite (001)

Johannes Lützenkirchen^{a,*}, Frank Heberling^a, Filip Supljika^b,
Tajana Preocanin^b, Nikola Kallay^b, Florian Johann^c, Ludger
Weisser^c and Peter J. Eng^d

DOI: 10.1039/b000000x [DO NOT ALTER/DELETE THIS TEXT]

We present a multidisciplinary study on the hematite (001) – aqueous solution interface, in particular the relationship between surface structure (studied via surface diffraction in the presence of a water film) and the macroscopic charging (studied via surface- and zeta-potential measurements in electrolyte solutions as a function of pH). Upon aging in water changes in the surface structure are observed, that are accompanied by drastic changes in the zeta-potential. Surprisingly the surface potential is not accordingly affected. We interpret our results by increasing hydration of the surface with time and enhanced reactivity of singly-coordinated hydroxyl groups that cause the isoelectric point of the surface to shift to values that are reminiscent of those typically reported for hematite particles. In its initial stages after preparation the hematite surface is very flat and only weakly hydrated. Our model links the entailing weak water structure with the observed low isoelectric point reminiscent of hydrophobic surfaces. The absence of an aging effect on the surface potential vs. pH curves is interpreted as domination of the surface potential by the doubly coordinated hydroxyls, which are present on both surfaces.

Introduction

The solid-aqueous solution interface is of interest in a wide range of scientific disciplines, including corrosion and corrosion inhibition¹⁻³, catalyst preparation⁴⁻⁶, colloid chemistry⁷⁻⁹, nanotechnology¹⁰⁻¹², geochemistry¹³⁻¹⁵, soil chemistry¹⁶⁻¹⁸, clay and clay mineral chemistry¹⁹⁻²¹, environmental chemistry²²⁻²⁴ etc., and overlaps thereof²⁵⁻²⁷. As a consequence many experimental and theoretical studies exist and highly detailed knowledge has been acquired from various points of views. Modern experimental techniques probe adsorbate structure²⁸, surface structure¹⁴ or interfacial water structure^{29, 30}. Theoretical work attempts to yield more insight in the sometimes difficult interpretation of such data³¹. Yet, several aspects still hamper the full understanding of the interfacial systems. One important aspect in that context is that the different scientific disciplines sometimes develop independently from each other. Correspondingly, discoveries or observations made in one discipline are not necessarily taken up in another. A further drawback is related to the fact that many studies include no more than one technique to gather experimental or computational data. While the comparison between experiment and theory is

[journal], [year], [vol], 00–00 | 1

This journal is © The Royal Society of Chemistry [year]

often included, the precise relation of various experimental results originating from different techniques is rather sparse. It is therefore important to establish more accurate links between experiments and models emerging from different techniques (macroscopic and structural) and simulations.

5 Some time ago we have reconciled the interfacial behaviour of α - Al_2O_3 (sapphire) single crystals with (001) orientation³² in order to find out whether and which of the available data can be understood in one phenomenological picture. This attempt required review of available literature including particular focus on the origin and treatment of the samples. It was finally postulated that the remaining data along with
10 our own could be understood by a dual charging mechanism. The reconciliation included data from non-linear optic techniques (sum frequency and second harmonic generation), streaming potential and colloid adhesion studies, contact angle experiments and surface complexation models all as a function of pH, which is a master variable for the oxide-aqueous solution interface. The dual charging
15 mechanism that allows to explain the experimental data involved the classical protonation and deprotonation of doubly coordinated aluminol groups which are the only surface hydroxyl groups on the ideal surface, plus a rather unconventional contribution from ion adsorption in the electr(ochem)ical double layer. The latter (besides being unconventional for the oxide-electrolyte interface community) has
20 been under hot debate for nearly a decade by now. It involves the physical adsorption of hydroxide ions and protons at interfacial water layers with a preference for the hydroxide ion. Strong adsorption of the hydroxide ion is assumed mostly by experimentalists³³⁻³⁸. However, others find that the proton is preferentially adsorbed³⁹, that the charge is negligible⁴⁰, or that there is no spectroscopic evidence
25 for hydroxide ions at the surface for very high NaOH concentrations or in the absence of an inert background electrolyte^{41, 42}.

An accepted generic feature is the occurrence of the isoelectric point (IEP) in aqueous solutions at pH 2 to 4 for surfaces as different as diamond, PTFE, oil, gases, gold etc.⁴³⁻⁴⁵ Unlike oxide surfaces, all these systems have in common the absence
30 of surface functional groups that could cause pH dependence. Without the occurrence of shifts in the IEP with changes in electrolyte concentrations and composition, experimentalists are left with only one solution to the problem that can explain the charge and the pH dependence at the same time. Even for ice surfaces the low IEP has been observed^{46, 47}. Especially in the case of ice this is surprising, as
35 one would expect the IEP to be where bulk water is neutral. The simplest interpretation of the low IEPs involves the hydroxide ion to be more strongly attracted to the interface than the proton or in other words that dissociation of water at interfaces is very different from dissociation of bulk water. On a similar note the charge of gas bubbles in pure water at pH 7 is argued to be due to the presence of
40 hydroxide ions at the interface in absence of a better explanation⁴⁸.

On oxide minerals the protonation and deprotonation of surface hydroxyls has been traditionally invoked to explain pH-dependent charging. The corresponding pK values are successfully predicted from the surface structure for well-defined particles⁴⁹⁻⁵². For various single crystal samples, the predicted pK values fail to
45 reproduce the experimentally observed IEP, which finally led us to postulate dual charging, involving the traditional picture of charged surface hydroxyls plus the unconventional charging of the adjacent water layer. According to the traditional picture, points of zero charge for most oxide particles should coincide in the absence of specific adsorption of background electrolytes and the corresponding
50 IEPs should be directly related to the pK values of the surfaces, i.e. at pH about 6 in the case of hematite (001) and sapphire (001)^{30, 53, 54}. Instead, the measured IEPs are at pH about 4, in the range of those observed for the “inert” surfaces discussed above. On sapphire (001) the predicted point of zero charge is confirmed in sum frequency generation studies³⁰ or contact angle investigations³², while the IEP of 4 is

found in other experiments^{53, 55}. Importantly, some of the seemingly contradictory results have been obtained on identical samples³². The difference can therefore safely be assumed to be real and can phenomenologically be explained by a dual charging mechanism.

5 On sapphire (001) both contributions to the dual charging mechanism (surface hydroxyls and water layer) arise from protons and hydroxide ions. The adsorption of protons to or the release of protons from the surface aluminols would classify them as surface charge/potential determining ions, whereby their contribution to charge accumulation is restricted to the plane of the surface hydroxyls. The second
10 contribution that arises from uptake of protons on or release of protons from adjacent water layers in turn affects the zeta-potential. In particular on surfaces like sapphire (001) the surface functional groups (involving only doubly coordinated oxygens) are rather stable and do not protonate or deprotonate within the usual pH-range.

15 Surfaces like silver halides on the other hand do not have the disadvantage that the same ions affect both surface and zeta-potential, and in particular protons and hydroxide ions do not affect the surface potential, which is controlled by silver and halide ions. In such systems simultaneous measurements of surface and zeta-potential clearly illustrate the difference between the action of the surface
20 potential/charge determining ions and the action of protons and hydroxide ions, which were found to influence the zeta-potential⁵⁶.

Furthermore, studies of both flat single crystals and colloidal particles showed, that hydroxide ion adsorption was more pronounced on the flat surfaces⁵⁷ in agreement with MD-simulations⁵⁸. Knowing both, surface and zeta-potentials, is therefore one
25 key to the understanding of flat interfaces with defined crystallographic orientation, which are often taken as model substrates to investigate contaminant uptake, dissolution, growth and other phenomena. In the case of sapphire^{32, 59}, we relied on surface potentials estimated from surface complexation modelling. For the silver halides both quantities were measured⁵⁷ thus avoiding model inherent assumptions.

30 A dual charging model was shown to reproduce all experimental observations qualitatively⁵⁷.

The present study tries to push the approach further by applying various experimental techniques to identical samples and investigating the effect of aging on the hematite (001) surface. There is some indication from previous second harmonic
35 generation and atomic force microscopy (AFM) reporting relatively low points of zero charge that this surface has unexpected properties similar to sapphire (001)⁶⁰. In those studies it was reported that annealing of the surface led to changes in the experimental results, but no conclusions about the origin of the changes were possible.⁶⁰ Direct zeta-potential measurements for hematite (001) are not available
40 to our knowledge but the hematite (001) surface has seen recent interest from various groups.

Surface diffraction is the major technique to study the structure of the surface and/or the adjacent water layer and to deduce which surface functional groups are present^{61, 62} and what kind of water structure forms at the interface²⁹. An important conclusion
45 has been that the water on annealed hematite (001) is weakly structured²⁹. Another conclusion was that a bi-domain structure persists at the surface where the contributions from both domains varied in the different studies^{61, 62}. In the remainder of the text we will discuss this bi-domain structure which had been observed by other methods^{63, 64}. The two distinct structures that emerged from these studies are
50 $O_3\text{-Fe-Fe-R}$ and $O_3\text{-Fe-O}_3\text{-R}$. How these terminations relate to the bulk hematite structure is displayed in Figure 1. For the oxygen terminated surface ($O_3\text{-Fe-Fe-R}$, Figure 1, left) the surface is comprised of doubly coordinated oxygen atoms. By removing the top oxygen layer the double iron termination ($\text{Fe-Fe-O}_3\text{-R}$, Figure 1, 2nd structure) is obtained. Further removal of an iron layer yields the single iron

termination (Fe-O₃-Fe-R, Figure 1, 3rd structure). The fourth option (noted O₃-Fe-O₃-R, Figure 1, right) is terminated by singly coordinated oxygen atoms. It may be understood as the Fe-terminated surface with water/hydroxide adsorbed to the top Fe atoms. This termination may form upon addition of Fe-ad atoms onto the oxygen termination⁶⁵, with subsequent rapid hydroxylation⁶⁶. The O₃-Fe-O₃-R-termination may as well be understood as an oxygen termination with iron vacancies in one of the top iron layers (indicated by transparent iron atoms in Figure 1, upper panel, right). It is important to note, that due to the low scattering cross-section of protons, surface diffraction does not allow to distinguish whether the top oxygen atoms are oxygen (O²⁻), hydroxide (OH⁻), or adsorbed water molecules (H₂O).

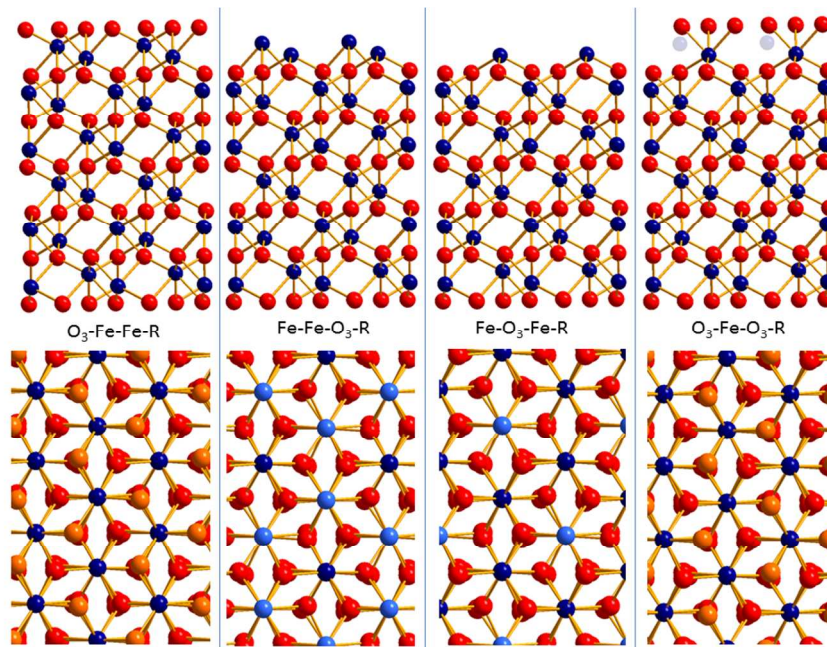


Fig. 1 A selection of chemically distinct surface terminations of hematite (001) (O: red, Fe: blue). The top panel shows side views of four possible terminations, the lower panel shows the corresponding top views. In the top views the surface atoms are highlighted in orange (oxygen) or light blue (iron).

Another series of studies involved surface potential measurements⁶⁷⁻⁷¹. The bulk part of the data suggests a broad plateau-like region in surface potential vs. pH curves with an increase at sufficiently low and a decrease at sufficiently high pH. Various interpretations of the data have been proposed. One interpretation was based on a shielding mechanism⁷¹, by which reactive groups could not be protonated or deprotonated, but this mainly explains the kinetics of the reaction and does not apply to our investigation. Two major difficulties appear in interpreting the experimental data: the determination of the point of zero surface potential and the absolute value of the surface potentials. The points of zero potential on two different hematite (001) samples have been fixed at the mid-pH of the plateau (suggesting a value of about 6)⁷⁰ or inferred from numerical procedures (resulting in a value of about pH 8.3)⁷¹. In our present work we combine CTR and surface potential data and include zeta-potential measurements. Thus we probe the surface structure and the concomitant surface potential as well as the water structure and the concomitant interfacial potential, which results from the net charge within the electrokinetic shear plane.

A second aspect addresses the aging of the hematite surface. To this end we have exposed the crystal to solutions for extended periods of times, and followed the changes with zeta-potential measurements. The initial (referred to as “fresh”) and final (referred to as “aged”) states were analysed by surface diffraction to generate a consistent picture between the structure of the interface and the concomitant charging properties. The measurements were all done on samples from the same source, treated in the same way and subject to similar time dependence. High resolution atomic force microscopy (AFM) on a fresh sample confirms various features of the surface diffraction study.

10

Experimental

Sample origin and preparation

15 The samples were purchased from “Surfacenet” (Münster, Germany). They are polished on one side and have dimensions of 10 mm times 20 mm. These samples fit exactly into the set-up used for zeta-potential measurements. Samples for surface potential measurements are smaller so that they allow the construction of a single crystal electrode. For the AFM study a 10 mm times 10 mm sample was used.

20 According to the supplier the single crystals are produced from a natural crystal. The exposed crystal face in all experiments is the polished (001) face. Samples are pre-treated according to a procedure previously established for sapphire (001)^{32, 59}, which has been used or adopted by others^{72, 73}. The samples are soaked in acetone overnight and subsequently washed by ethanol and finally by MilliQ water. On

25 sapphire (001) this procedure ensures elimination of organic contamination and reproducible results from streaming potential measurements.

Solution preparation and measurement conditions

All solutions are prepared from MilliQ water (18.2 MΩcm) and chemicals are all from Merck. Solutions are kept under Argon during all measurements (in the surface diffraction measurements under Helium) to minimize intrusion of carbon dioxide. pH titrations are started at high pH. pH is subsequently decreased by adding acid.

Zeta-potential measurements

35 Zeta-potential measurements are done as previously described in detail^{32, 57, 59, 74}. We use the SurPass Electrokinetic Analyzer (Anton Paar, Graz, Austria) to carry out the experiments. In short, two samples are glued with the unpolished side to two stamps. The exposed polished side is rinsed by ethanol and MilliQ water and then the stamps

40 are inserted into a cell to create a rectangular flow channel. The channel width is adjusted to about 100 μm. A titration is started using a solution of a given electrolyte concentration (NaCl), in which the pH is increased by adding NaOH (50 mM) and then a titration is started by adding HCl (50 mM). Equilibration times are at least 10 minutes per point and at least 4 replicate measurements are performed at

45 each pH. pH measurements in the SurPass set-up are performed using the built-in device, which is calibrated against three buffer solutions. All measurements are done at room temperature.

After the first series of measurements the samples are kept in an aqueous environment (MilliQ water). Subsequent measurements surprisingly led to strong

50 shifts in the zeta-potential. This is unlike observations with sapphire (001) where the charging behaviour can be reproduced over extended time periods with a given set of *unannealed* samples.

Surface potential measurements

Surface potential measurements are performed as previously described⁷⁰. The potential of the Single Crystal (SCr)-hematite electrode is measured by a Metrohm 713 pH-meter. A silver/silver chloride electrode, filled with 3 mol dm⁻³ KCl solution, with a salt bridge (Metrohm, 6.0729.100) filled with sodium chloride ($c = 10^{-3}$ mol dm⁻³), is used as a reference. pH is measured using a combined Metrohm glass electrode (Metrohm, 6.0259.100). The pH-meter is operated by batteries (Metrohm, 826) and used for the measurements of pH values. Systems are thermostated at 25.0 °C. The experiments are performed under argon atmosphere.

The measuring system (thermostated vessel, electrodes, magnetic stirrer) is placed in a Faraday cage. The surface of the SCr-hematite electrode is cleaned with ethanol and rinsed with water before all measurement runs (i.e. beyond the standard cleaning procedure). Sodium chloride ($c = 10^{-3}$ or 10^{-2} mol dm⁻³) is used as background electrolyte. Potentiometric titrations are performed by adding hydrochloric acid ($c = 10^{-1}$ mol dm⁻³) or sodium hydroxide ($c = 10^{-1}$ mol dm⁻³). Time intervals between additions are between 10 minutes and 15 minutes. Potentiometric titrations run entirely automated. Data are collected every four seconds.

20

CTR-data collection

Crystal truncation rod (CTR)-data are recorded at the Advanced Photon source at Sector 13 (GSECARS) at the 13 BMC station.

The samples used for collection of CTR-data include a fresh sample and an aged sample that had been retained from the last series of zeta-potential measurements. Beamline optics contain a focusing SI (111) double crystal monochromator. The photon energy is fixed to 15 keV. The sample is oriented relative to the beam on a Newport 2+2+kappa diffractometer. Measurement of the specular CTR is performed with the surface normal of the sample in a horizontal position, while for the measurements of the off specular CTRs the incident angle of the beam relative to the surface is maintained at a constant value of 2°. The diffraction signal is recorded by a PILATUS 2D pixel array detector with 195 x 487 pixels (vertical x horizontal). The size of the beam spot at the sample surface is limited by horizontal and vertical slits to 500µm x 500 µm (vertical x horizontal).

The sample is mounted onto the diffractometer in an environmental sample cell, which is constantly flushed with humid He-gas in order to maintain the sample surface fully hydrated during the measurements.

CTR-data integration

Integration of diffracted intensities from the PILATUS images is performed using the tdl software package (<https://github.com/xraypy/tdl>).

A total of 692 and 654 structure factors are recorded for the fresh and the aged hematite samples, respectively. The measured structure factors are averaged in the p3m plane group, resulting in 524 and 439 unique structure factors, respectively. Note that a single hematite (001) termination exhibits p3 symmetry only. However, in the hematite unit cell there exist 6 chemically equivalent terminations, which are crystallographically distinct, but equally likely to constitute the actual surface. These terminations are linked by the threefold symmetry axis along hematite [001] and the glide plane symmetry along the same axis (space group R-3c). As the surface structure is modelled assuming an equal abundance of these symmetry related domains at the surface, as in previous studies^{61, 62}, the total symmetry considered for hematite (001) CTR data reduction may be increased from p3 to p3m without any loss of information. This reduces the number of unique structure factors

and, correspondingly, reduces the computational effort during modelling.

CTR-data modelling approach

Data modelling is performed using a modified version of the python interface structure refinement package (<https://github.com/xraypy/tol>). The modified version was expanded to allow for the treatment of multiple surface terminations and symmetry related surface domains, following an approach described earlier⁷⁵. The abundance of chemically distinct surface terminations is thereby adjusted as a fitting parameter during data modelling, while an equally weighted average is taken over the symmetry related domains. Symmetry related domains and surface terminations are summed in a coherent fashion. In agreement with previous studies^{61, 62}, incoherent summation did not yield acceptable fits to the data.

Preliminary modelling approaches, using a single surface termination, failed to describe the data for both samples by a simple stoichiometric surface termination. Occupancies of the surface iron sites rather indicated a surface termination consisting of a mixture of O₃-Fe-Fe-R and O₃-Fe-O₃-R domains very similar to previous results^{61, 62}. In our modelling approach we therefore started with a linked two domain model as reported by Trainor et al.⁶², where the O₃-Fe-Fe-R and O₃-Fe-O₃-R domains share common structural parameters in layers that are not directly exposed to the surface or mimicking adsorbed water molecules (modelled as oxygen atoms, because of the low x-ray scattering cross-section of hydrogen). In contrast to Trainor et al.⁶² and Tanwar et al.⁶¹ this "linked model" did not yield a satisfactory description of the CTR data ($\chi^2 > 5$) for both data sets. Therefore, after the initial adjustment of the linked model, the structural parameter space was limited to a narrow range around the common value (± 0.005 in fractional coordinates) and the model was readjusted with individual parameters for both domains.

All atom displacements are modelled such that the threefold symmetry of the surface structure is maintained. The iron atoms have fixed lateral positions as they sit on the threefold symmetry axes. The vertical displacement of the oxygen atoms in one layer is described by one parameter fixing the oxygen atoms at equal vertical positions. Lateral positions of the three oxygen atoms in one layer are described by two parameters (e.g.: O₁: (x, y), O₂: (-x+y, -x), O₃: (-y, x-y)) to keep the symmetry.

During the model adjustment the bond valence sums of the iron atoms in the surface structure according to Brown and Altermatt⁷⁶ are constrained to stay within 5% of the nominal iron valence of +III. The bond valence calculations on the surface oxygen atoms simultaneously yield information, which can be used to draw conclusions about their protonation states.

AFM measurements

High resolution AFM measurements are carried out using a Cypher ES apparatus (Asylum Research). Both imaging and force spectroscopy are performed in AC mode with an "Arrow UHF AuD" cantilever from NanoWorld. The cantilever is excited using blueDrive photothermal excitation with oscillation amplitudes < 1nm in liquid environments and < 5nm in air. The fresh sample is studied to gain insight in the roughness of the sample and to try to support results from the CTR study concerning surface structure of and interfacial water structure on the fresh sample.

Surface complexation modelling

Surface complexation modelling is done with a modified version of FITEQL2. The surface and zeta-potential data are fitted to a set of surface chemical equations involving a model for the electrical double layer (see SI).

Results and discussion

Zeta-potential measurements

Figure 2 shows the pH function of the zeta-potential as it changes from the fresh sample to a steady state (aged sample). The initial state of the surface produced repeatedly an IEP of about 4. Later, the IEP shifted gradually to higher pH until it reached a steady state value of about pH 9.

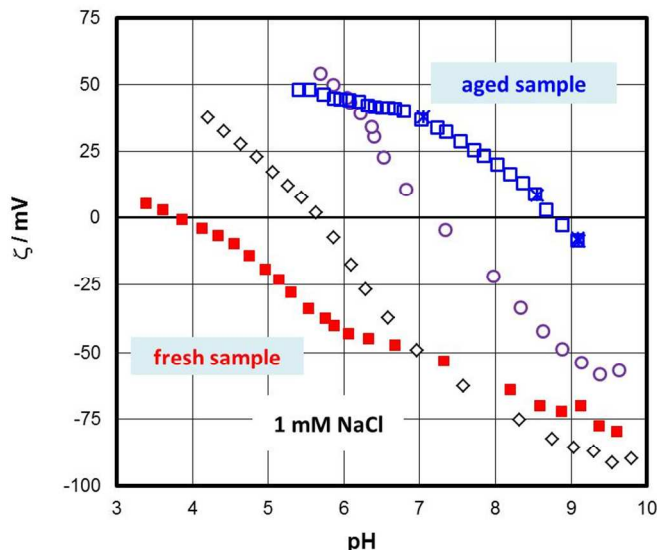


Fig. 2 The effect of aging in aqueous solution on the Zeta-potential of the hematite samples measured in 1 mM NaCl solution.

10

The initial IEP obtained for the fresh sample is identical to the ones routinely
 15 obtained for “inert” surfaces⁷⁷, but also for isostructural sapphire (001) samples⁷⁸ or
 even flat samples of TiO₂⁷⁹ or ZnO⁸⁰. The occurrence of this IEP for so many
 different samples could be challenged in the sense that it is triggered by the method
 or by systematic errors or artefacts. For sapphire (001) the IEP of about 4³² has been
 interpreted in terms of charging of the interfacial water layer adjacent to the surface.
 20 Weak ordering of water at both sapphire- and hematite (001) surfaces²⁹ supports this
 interpretation. The observation of an IEP at about pH 9 for the aged hematite
 sample, i.e. identical to the bulk of IEPs for hematite particles, suggests that the
 method is not at the origin of those results. The transient change could be due to
 structural changes at the surface of the sample and/or changes related to the
 25 interfacial water structure.

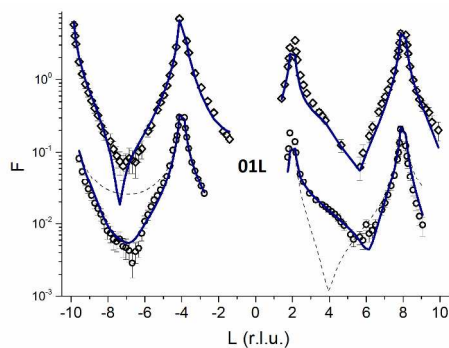
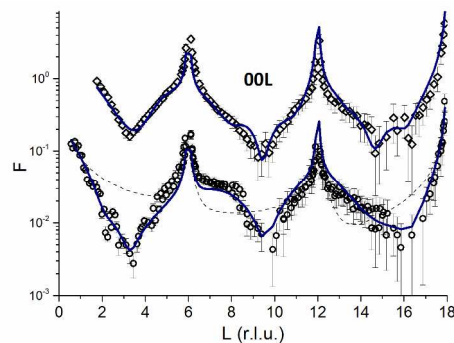
Surface potential measurements

The surface potential vs pH response was not prone to significant changes even for
 an extended period of time. We always observe the same overall features with a

broad range of constant potentials at pH values between 4 and 9. This plateau-behaviour can be explained by the MUSIC model as previously discussed^{67, 70}. Briefly, the doubly coordinated surface hydroxyls are rather inactive towards protonation and deprotonation since their pK values are about 0 and 12⁵⁴. The insensitivity of the surface potential vs. pH curves to aging confirms our previous claim that a surface with the plateau like behaviour is the thermodynamically stable one.⁷⁰

Surface diffraction data

CTR-data and best fit model calculations are shown in Figure 3. As an example the 00L rod (top panel in Figure 3) indicates that the surface diffraction data change with time. Clearly between $6 < L < 9$ a shoulder is present on the fresh sample that disappears on the aged sample.



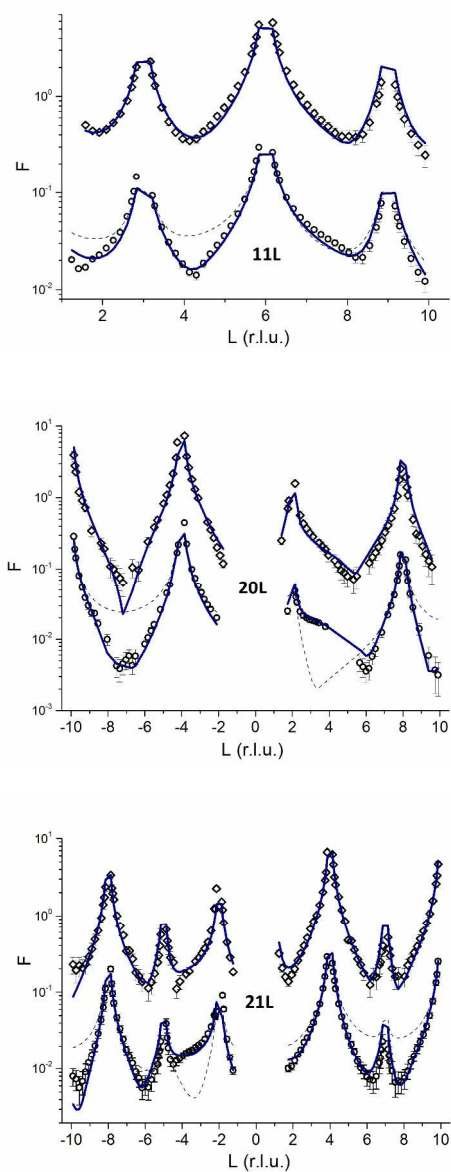


Fig. 3 CTR data for the aged (upper graphs, diamonds) and fresh (lower graphs, circles) are shown along with calculated structure factors (solid lines). The thin dashed lines in the lower graphs indicate the structure factors expected for bulk terminated hematite. The data for fresh and aged hematite are offset for clarity.

5

The comparison with the bulk terminated hematite (dashed lines) shows that the real surfaces are different from the ideal surface. The full lines correspond to the structural models for the two samples obtained in the present study. The agreement between experiment and model is rather good ($\chi^2 = 3.97$ and $\chi^2 = 2.97$ for the fresh and aged samples, respectively). Both surfaces are bi-domain, with different contributions from the two terminations.

The structural parameters corresponding to the best fit models are reported in supporting information (Table S11 for the fresh hematite sample and in Table S12 for the aged hematite sample). For comparison, the structural coordinates of the bulk terminated hematite structure are given in Table S13. Ball and stick representations of the best fit structures for both surfaces are shown in Figures 4 and 5. The z-offsets between the two domains in the structural pictures are artificial (only for illustration). The patchwise distribution is probably real, but the dimensions of the patches cannot be quantified from the CTR-data. The fact that only coherent addition of the contributions from the two terminations yield reasonable fits to the data, points, however, towards a small scale mixing of the domains. Interestingly, AFM images of the fresh surface (to be discussed below) support the patchwise structure and even a recent theoretical study suggests that the patchwise organisation is energetically favourable⁸¹.

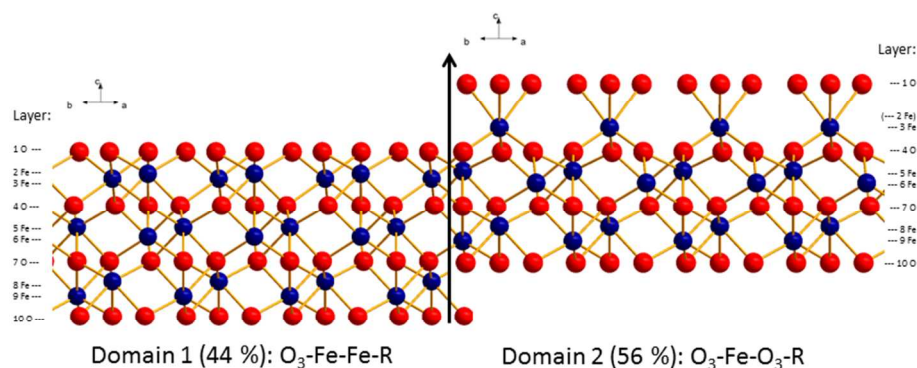


Fig. 4 Best fit structural model for the surface of the fresh hematite sample (oxygen: red, iron: blue). Indicated are the domain and layer nomenclature as used in Table S11.

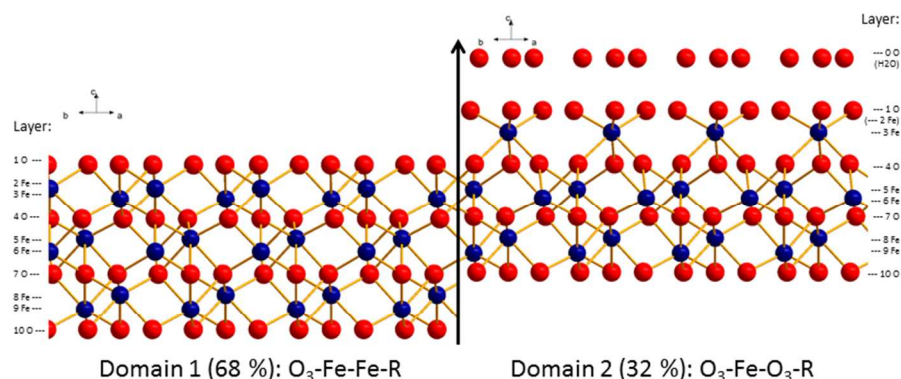


Fig. 5 Best fit structural model for the surface of the aged hematite sample (oxygen: red, iron: blue). Indicated are the domain and layer nomenclature as used in Table S12.

5 From Figures 4 and 5, it is clear that the contribution of domain 2 has decreased upon aging. Furthermore, the distances between the top oxygen atoms and the first iron layer on domain 2 is dramatically different. Finally on the aged sample a water layer is found, which in the sketch is shown over domain 2 for illustrative purposes only, since such information cannot be obtained from the CTR model. The
 10 occupancy in the water layer is relatively low (~20% of a mono layer), suggesting stronger ordering than for the fresh sample, but clearly not very the very strong ordering found on other cuts of hematite.²⁹

Table 1 shows a compilation of the structure relaxations observed at the hematite (001)-water interface in this and in previous CTR^{61, 62} and X-ray reflectivity²⁹
 15 studies. DFT results by Trainor et al.⁶² are listed for comparison.

From a qualitative comparison some remarkable similarities exist. For the O₃-Fe-Fe-R termination (domain 1) the topmost oxygen layer relaxes away from the underlying iron layer (1 O₃ - 2 Fe). The two iron layers 2 Fe and 3 Fe contract. This contraction extends in most experimental observations (except Tanwar et. al.⁶¹) to the iron layers underneath (5 Fe - 6 Fe). The iron layers are marked in boldface in
 20 Table 1. The Fe-Fe contraction also emerges for the 5 Fe and 6 Fe layers in the O₃-Fe-O₃-R termination. For the O₃-Fe-O₃-R termination two different trends concerning the relaxations of the topmost layers occur. For the aged hematite in this study, the annealed hematite by Trainor et al.⁶², and in nice agreement with DFT
 25 results by Trainor et al.⁶², the top oxygen layer (1 O) contracts towards the 3 Fe layer, while the 3 Fe - 4 O₃ and 4 O₃ - 5 Fe layers expand.

Table 1 Comparison of structure relaxations (percent difference between interlayer distances of the relaxed and the bulk structure) at the hematite(001)-water interface in this and previous studies.

layer	Bulk-interlayer distance	this study – CTR aged hematite	Trainor ⁶² - CTR	Trainor ⁶² - DFT	Catalano ²⁹ - XR	Tanwar ⁶¹ - CTR unreacted sample	this study CTR fresh hematite
Panel 1: O ₃ -Fe-Fe-R termination							
Domain abundance		68 %	62 %	-	100 %	54 %	44 %
1 O ₃ -2 Fe	0.844	16	23	35	34	1	5
2 Fe-3 Fe	0.604	-28	-48	-41	-17	-18	-67
3 Fe-4 O ₃	0.844	-1	13	12	7	4	31
4 O ₃ -5 Fe	0.844	-3	2	2	1	1	8
5 Fe-6 Fe	0.604	-12	-6	6	-22	0	-35
6 Fe-7 O ₃	0.844	9	5	-4	7	3	19
7 O ₃ -8 Fe	0.844	2	0	0	7	-1	-3
8 Fe-9 Fe	0.604	0			-6	0	0
9 Fe-10 O ₃	0.844	0			1	-1	0
Panel 2: O ₃ -Fe-O ₃ -R termination							
Domain abundance		32 %	38 %	-	0 %	46 %	56 %
1 O ₃ -3 Fe	1.448	-38	-24	-28	-	2	20
3 Fe-4 O ₃	0.844	58	19	20	-	1	14
4 O ₃ -5 Fe	0.844	26	24	26	-	1	-11
5 Fe-6 Fe	0.604	-38	-48	-69	-	-18	-23
6 Fe-7 O ₃	0.844	-7	12	15	-	4	10
7 O ₃ -8 Fe	0.844	7	0	0	-	1	-3
8 Fe-9 Fe	0.604	4			-	0	-4
9 Fe-10 O ₃	0.844	-6			-	3	2

5

Deviating from this trend, the structure reported by Tanwar et al.⁶¹ seems to be an intermediate case, while for the fresh hematite sample in the present study we observe an opposite relaxation of 1 O₃ away from 3 Fe.

10 Based on the CTR results in this study an explanation for the relaxation of 1 O₃ away from 3 Fe on the fresh hematite sample, might be significantly weaker hydration of the surface of the fresh hematite sample compared to the hydration of the aged hematite sample. The surface hydration of the two samples is best compared by regarding the electron density distribution of the surface structures projected onto the surface normal (Figure 6).

15

For the aged hematite sample Figure 6 shows a peak for the partially occupied adsorbed water layer (~20 % of a mono layer) at $z = 16 \text{ \AA}$ and a relatively well structured first bulk water layer ($z(\text{water}) = 18.25 \text{ \AA}$, $U_0 = 0.039 \text{ \AA}^2$). The interlayer distance between

[journal], [year], [vol], 00–00 | 13

consecutive bulk water layers is, however, small ($d(\text{water}) = 0.81 \text{ \AA}$) and the increase in the vibrational distribution from layer to layer is relatively large, $\bar{U} = 0.45 \text{ \AA}^2$, indicating that bulk water layers beyond the first layer are not structurally resolved. The bulk water model used here is identical to the one presented by Fenter and Sturchio (2004)¹⁴.

5 For the fresh hematite sample good fits to the data could only be obtained without considering distinct adsorbed water molecules. The bulk water profile included in the best fit model is unstructured. Furthermore, it is so far above the surface that it may not be physically reasonable. The improvement of the model fit by including
 10 numerically significant effect and improves the goodness of fit from $\chi^2 = 4.29$ ($p = 37$) to $\chi^2 = 3.97$ ($p = 41$). Best fit bulk water parameters are: $z(\text{water}) = 20.62 \text{ \AA}$, $U_0 = 1.3 \text{ \AA}^2$, $d(\text{water}) = 1 \text{ \AA}$, and $\bar{U} = 0.4 \text{ \AA}$.

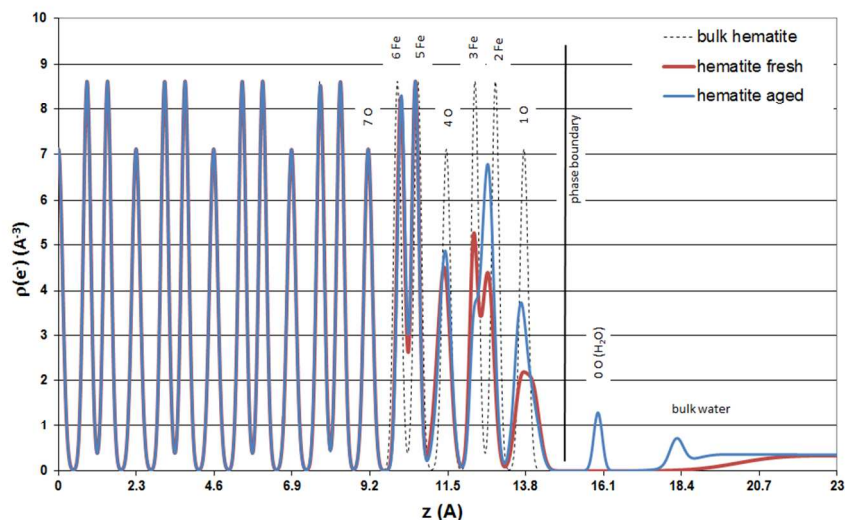


Fig. 6 Electron density distribution according to the hematite (001) surface structures of bulk hematite (dashed line), the fresh hematite sample (thick red line), and the aged hematite sample
 15 (blue line), projected onto the surface normal. The origin marks the arbitrary transition between undisturbed bulk and surface structures. The thick black line labeled “phase boundary” is placed between the terminating oxygen atoms (O^{2-} , OH^- , or H_2O) and the adsorbed water. It is not more than a guide to the eye, since the position is somewhat arbitrary.

Comparison of the relative abundance of the two reported surface domains (reported in
 20 Table 1) reveals an interesting trend. Upon chemical mechanical polishing the abundance of the two domains is similar (44/56: fresh hematite in this study, 54/46: unreacted hematite in Tanwar et al.⁶¹). Prolonged aging in aqueous solution (aged hematite, this study) as well as mild annealing (8 times 30 min at 600°C ⁶²) favors the formation of the $\text{O}_3\text{-Fe-Fe-R}$ termination. Only upon extensive annealing (12 h at 1100°C) a fully $\text{O}_3\text{-Fe-}$
 25 Fe-R terminated hematite was inferred²⁹. This agrees with the stability trends reported by Trainor et al.⁶² based on DFT calculations. These indicate that the $\text{O}_3\text{-Fe-Fe-R}$ termination is more stable than $\text{O}_3\text{-Fe-O}_3\text{-R}$ at elevated temperatures in dry environments e.g. during annealing. Furthermore, the stability of the $\text{O}_3\text{-Fe-Fe-R}$ termination is slightly favorable compared to $\text{O}_3\text{-Fe-O}_3\text{-R}$ at room temperature in aqueous environments. This
 30 agrees well with the observed evolution of the surface termination of hematite from 44% $\text{O}_3\text{-Fe-Fe-R}$ on fresh hematite to 68% $\text{O}_3\text{-Fe-Fe-R}$ on the aged hematite sample.

The evaluation of the surface diffraction data does not include hydrogen atoms. However, the surface is expected to be rapidly hydroxylated⁶⁶. Cutting the surface during its manufacturing will result in some termination exposing iron and/or oxygen. To include hydrogen atoms and concomitant role of interfacial water, we use a bond valence analysis based on the CTR results. The bond valence analyses of the fresh and aged surfaces show some differences. The bond valence for the various doubly coordinated oxygen atoms differs by no more than about 0.2 valence units, i.e. there is no significant difference. The undersaturation of the doubly coordinated oxygens is about one valence unit and addition of one proton would satisfy the oxygen valence for both fresh and aged hematite. This supports the view that these oxygen atoms are neither protonated nor deprotonated at the conditions of the CTR measurements. However, concerning the singly coordinated oxygen atoms, the fresh hematite sample exhibits an undersaturation by 1.75 valence units. The simplest way to reduce this deficit is to assume that the group is doubly protonated and has originated from adsorption of a water molecule at the iron termination⁶⁶. This would result in a stable, aquo-group terminated configuration and might remain non-reactive (as is concluded later to explain the zeta-potential data). In turn, on the aged sample the undersaturation of the singly coordinated oxygen is about 1.45 valence units. In that case two adsorbed protons would not allow a stable configuration. A more likely explanation is therefore interaction with water to yield a hydroxyl group and involve hydrogen bonding between neighboring hydroxyl groups or with adjacent water molecules. This would explain the presence of structured water on the aged surface.

Surface complexation modelling

For the following it has to be mentioned that CTR data have not been collected at various pH conditions or even in the presence of salt. Also the amount of water in our study is much lower than in the work by Catalano²⁹. A future comprehensive study should cover such aspects in order to test some of the model assumptions that will be used in the following.

30

Fresh hematite (001)

Figure 7 shows the surface- and zeta-potentials of the fresh sample. The surface potential exhibits the broad flat response in the mid pH-range that is believed to be due to the pK values of the doubly coordinated hydroxyl groups as discussed above. The point of zero charge of the sample would therefore be at pH about 6.5, close to the value reported for sapphire (001) based on sum frequency generation data³⁰. The surface-potential curves appear to exhibit an ionic strength influence similar to observations by Boily et al.⁶⁷ The zeta-potentials in turn exhibit an IEP at about pH 4, which appears to decrease with decreasing sodium content. The dual charging mechanism therefore needs to be involved to explain the data that have been obtained on identical samples.

Based on the CTR data, the iron-terminated surface is dominant on the fresh sample. Figure 3 shows schematically the presence of two domains. These are not separated by big distances. High resolution AFM (Figure 8) indicates that the surface should rather be imagined as a mix of small 10 to 30 nm patches of the two domains. The CTR data do not show significant water structuring. This could explain behavior similar to hydrophobic/inert surfaces. This agrees with previous studies by Catalano who found

[journal], [year], [vol], 00–00 | 15

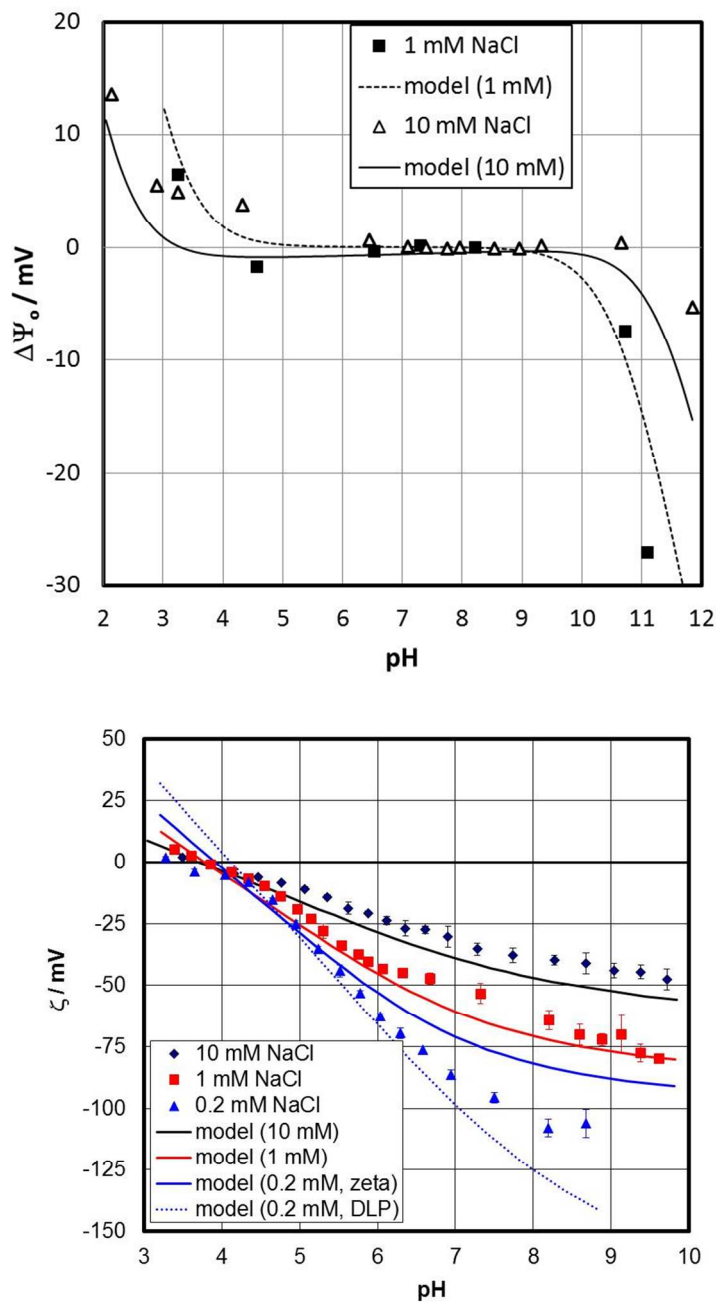
weak water ordering on hematite (001)²⁹. Catalano involved a thin water film in his work so that his results cannot be directly compared to our study, but in a qualitative way between the fresh and the aged sample the fresh sample surface clearly exhibits weaker water structuring.

5 In contrast to the macroscopic data, there is no salt present in the CTR study. Since the measurement campaign new evidence has appeared that related faces (the gibbsite basal plane) cause adsorption and layering of background electrolyte ions in CaCl₂-solutions at pH 6⁸². This was clearly shown by both AFM force curves and their interpretation in terms of electrostatic potentials and direct imaging for a 2:1 electrolyte. Even for KCl
10 and NaCl an increasing positive potential was reported for the gibbsite basal plane. Own, unpublished surface potential data for sapphire (001) support the adsorption of KCl. At constant pH of about 6 the surface potential increases with increasing KCl concentration. Finally, the presence of salt hydrates had been previously postulated based on XPS
15 studies on hematite particles, where in particular with increasing contributions from basal planes an enhanced presence of salt hydrates was reported⁸³. Based on the above, our present model approach for the fresh surface includes the following features:

- protonation/deprotonation of the surface hydroxyls (based on MUSIC type calculations^{52, 54}) to account for the conventional picture of oxide-aqueous solution interfaces (no attempt was made to relate pK values directly to the
20 CTR results, the values are in the expected and previously reported range)
- adsorption of NaCl within the Stern plane to account for the experimental evidence on this phenomenon at gibbsite basal planes and hematite particles
- adsorption of protons and hydroxide ions beyond the NaCl plane to account for
25 the pH dependence of the zeta-potential and the observed isoelectric point that is typically found for inert surfaces
- singly coordinated groups are assumed to be inert due to weak interaction with water as inferred from the CTR data

A sketch of the interfacial model is given in the Supplementary Information (Figure SI1) and the model parameters are given in Table SI4. Interestingly, simple versions of the
30 model, including only one or two of the above mechanisms failed to reproduce the experimental data.

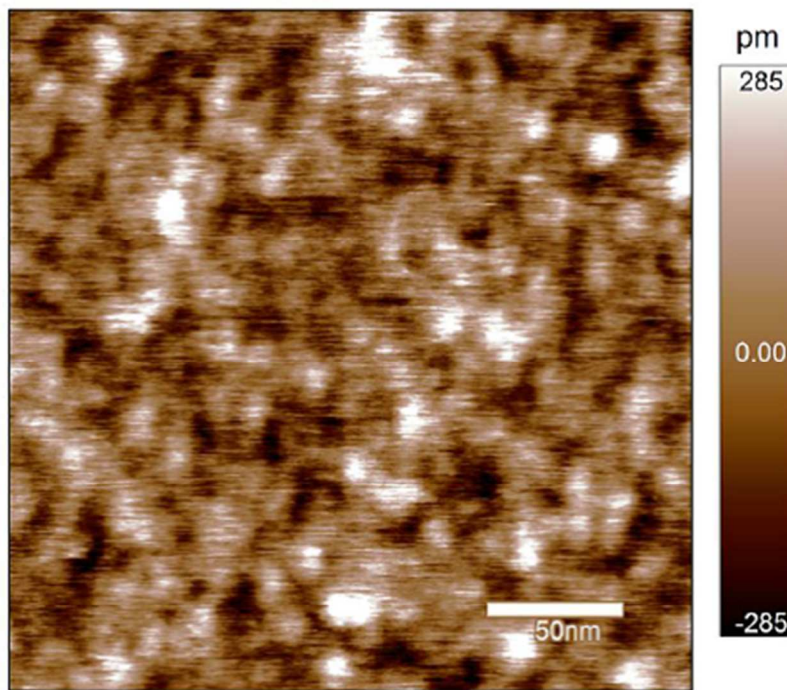
Lines in Figure 7 show the fit to the surface- and zeta-potential based on the model described above. The surface potential is well described and the inclusion of the salt interactions allow shifts in the surface potential curves with salt content to be described.
35 The traditional picture does not involve a significant effect of background electrolytes on the surface potential^{56, 57} and conventional surface complexation models agree with this⁵⁷.



5 **Fig. 7** Surface (top)- and zeta(bottom)-potentials for the fresh hematite- (001) sample. Symbols are experimental data and lines are calculated by the proposed surface complexation model. In the lower graph, two model lines are plotted for the 0.2 mM NaCl data. The one noted “zeta” points to the model-inherent slip plane distance, while the one noted “DLP” pertains to the potential at the onset of the diffuse layer.

The surface potential cannot be measured on an absolute scale and is therefore plotted as the difference ($\Delta\Psi_0$) to an arbitrary reference potential. The model inherent surface potential is affected by the salt level assuming adsorption of NaCl within the Stern plane. Diffuse layer potential data on gibbsite (positive in the absence of salt) show that addition of NaCl or KCl increases the potential⁸². Macroscopic data on gibbsite have been interpreted by adsorption of sodium and chloride on the basal plane, involving (unlike our model) protons⁸⁴. Spectroscopic data for gibbsite agree with the adsorption of both sodium and chloride at low pH⁸⁵. Even for hematite particles, such evidence has been presented.⁸³ The relative change of the surface potential as a function of pH is well described by the model. For the zeta-potential the slip-plane separation is the most important parameter involved. The good description of the zeta-potentials is to a large extent due to its adjustment. At the lowest salt content, the experimental data at high pH are between the potential with the assumed slip-plane separation (full line) and the one at the onset of the diffuse layer (dashed line). We involve a slip plane distance parameter that is related to the ionic strength (see SI for more detailed information). An individual adjustment of the slip plane distance would yield an even better fit to the data.

Whatever option is chosen, the model is in the correct range of potentials. At low pH, at the smallest salt content, the misfit between experimental and simulated zeta-potentials is largest. Under these conditions the ionic strength is not constant, since the addition of acid starts affecting the overall value. Therefore, we have carried out calculations with the correct concentrations of all components. This shifts the model for nominal 0.2 mM concentrations towards the one for 1 mM thereby decreasing the misfit; while the shift of the IEP is not reproduced. Overall, the results warrant additional CTR-investigations in the presence of NaCl.



25

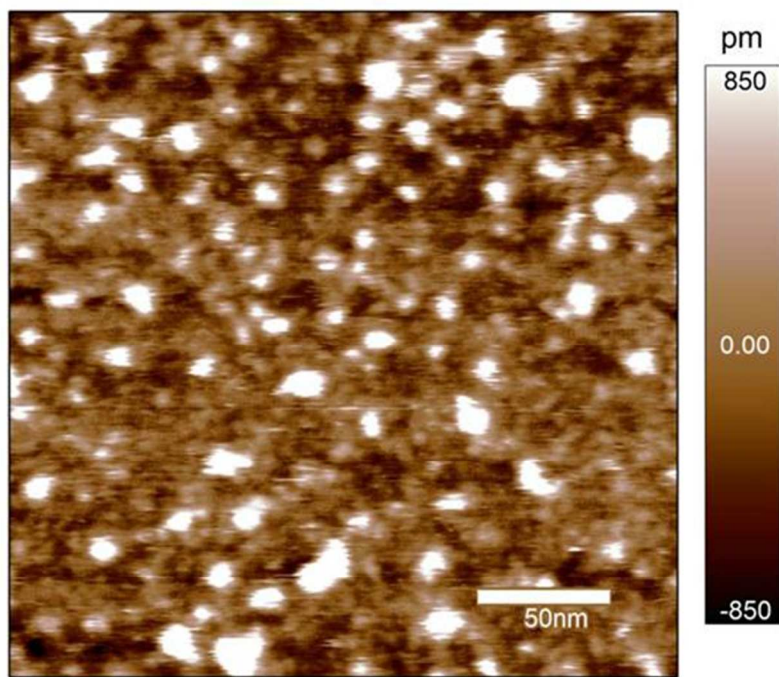


Fig. 8 High resolution AFM image of the fresh sample in air (top) and in water (bottom).

High resolution AFM does not show clear terraces on the fresh sample surface in air. However, the root mean square roughness is estimated to be 1.2 \AA under these conditions (Figure 8, top), comparable to the result from the CTR-study (1.1 \AA), i.e. very low. The various small areas/patches might correspond to the two domains that were discussed in the context of the CTR-data. Addition of water increases the roughness to between 3.9 and 4.4 \AA , addition of 1 mM KCl solution further increases it to 5 to 7 \AA . The addition of aqueous solutions at pH about 6 thus has a significant effect on the roughness (Figure 8, bottom) but this effect has not been observed in our CTR experiments. For resolution of hydration water layers⁸⁶ or adsorbed ions or ion layers our sample is probably too rough. However, we believe that sufficient circumstantial evidence⁸²⁻⁸⁴ exists by now that salt layers are present in related systems, as well as in expectedly different systems. Correspondingly, the assumption of salt in the Stern layer on hematite (001) is considered reasonable.

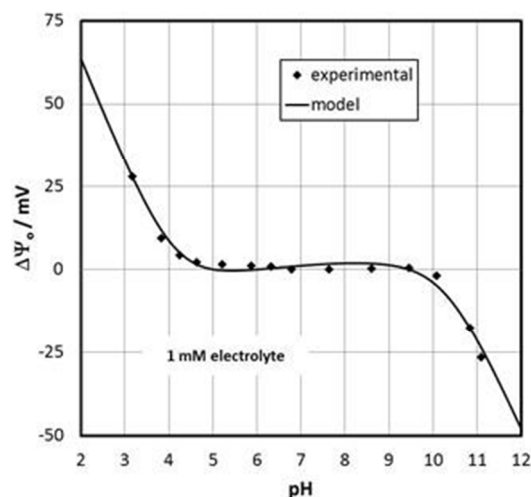
Force curves with a negative tip probe at pH 6 (not shown) were always repulsive in water and 1 mM KCl supporting the zeta-potential measurements for the fresh sample. Additional measurements in 1 mM HCl also produced repulsive interactions, in line with the shift of the IEP that occurs with decreasing sodium concentration (Figure 7). In 1 mM HCl potassium/sodium ions are absent and cannot contribute to the charging of the surface so that a “salt” layer cannot form.

Our surface complexation model does not need to resort to iron-surface species similar to acidic groups invoked for sapphire (001) to explain the low isoelectric point⁵⁵. We rely on the CTR-data in this respect and our model is able to describe the system very well on

that basis. We note that many parameters are involved, but most of them have been taken from associated systems (such as hydroxide adsorption on inert surfaces or expected protonation/deprotonation constants of the surface hydroxyls).

Aged hematite (001)

- 5 Based on the CTR data, the oxygen-terminated surface ($O_3\text{-Fe-Fe-R}$) is dominant on the aged sample. This supports a previous study where an annealed sample had been left to age and developed a surface potential response that was interpreted in terms of oxygen-termination⁷⁰. The measured surface potentials of the present sample indeed show the same response (for both fresh and aged states), while the zeta-potentials evolve with time
- 10 (Figure 2). The IEP of the aged sample is at about pH 9 at the steady state condition, which is similar to that measured on particles⁸⁷. Compared to the data for the fresh sample, the CTR data for the aged sample show adsorbed water molecules and the presence of a water film. This might suggest that the surface rearrangement is related to an increasingly pronounced interaction with water. In this interpretation the singly-
- 15 coordinated hydroxyl groups would interact more strongly with the interfacial water and would be able to affect the electrokinetic potentials substantially. Surprisingly, the experimental data suggest that these reactive groups do not contribute to the measured surface potential. In a model the singly-coordinated groups could be treated as adsorbates⁶⁵. This would be in line with a previous study on sapphire (001)⁸⁸, where the
- 20 intentional addition of dissolved aluminum caused a strong shift of the isoelectric point, similar to the present case. The action of the water can be held responsible for the difference between the fresh and aged samples. Another issue could be how the ad-atoms are distributed over the full surface. But this cannot be inferred from our data. No high resolution AFM images are available for the aged samples.
- 25 The results in Figure 9 show that the proposed model is capable of describing the surface (Figure 9, top) and zeta (Figure 9, bottom)-potentials in an excellent way.



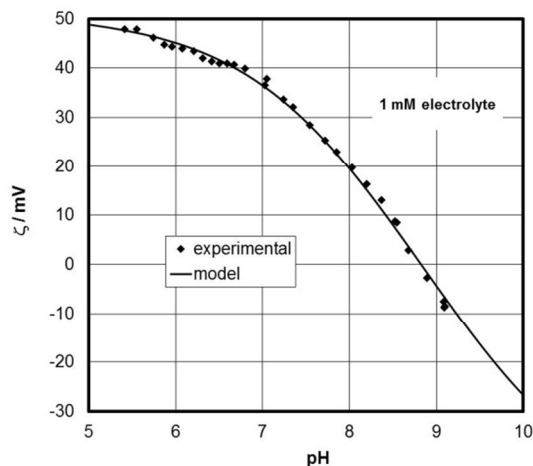


Fig. 9 Surface (top) and zeta(bottom)-potential for the aged hematite-sample, and model based on the concept and parameters given in SI.

5 The data for the aged hematite provide the first experimental observation via streaming potential measurements of an IEP around 9 for a flat oxide surface that would be expected based on the available data for particles that are established with far more popular methods, such as electrophoresis or acoustophoresis. The low IEPs previously reported for many oxide single crystals^{79, 80} have raised suspicion⁸⁹, since they do not
 10 obey “surface chemistry” in terms of the MUSIC model and because they are rather generic similar to hydrophobic/inert surfaces. It is interesting to note that the model for the aged hematite (001) surface produces the slight increase of the surface potential with increasing pH within the plateau region, which has been observed previously⁷¹, and which so far lacked an explanation.

15

Summary of the surface complexation models

Despite the surface characterization of the two samples, a substantial number of assumptions is involved in the model design. The following points address weak aspects of our modelling:

- 20
- The assumption about the reactivity of the singly coordinated groups is ultimately linked to the outcome of the zeta-potential measurements. In particular on the fresh surface inclusion of the singly coordinated groups would not allow a low isoelectric point to be modelled. The main argument is the lack of water interaction in the sense that a strongly ordered water film is not

25

 - The salt layering is unconventional in the sense that it does not involve proton co-adsorption (for chloride adsorption) or proton release (for sodium adsorption) unlike the model proposed by Rosenqvist et al.⁸⁴

30

 - The major parameter for describing the zeta-potential is the slip-plane separation. We currently have to consider it as a pure fitting parameter, but we

expect that in the future with the advent of new techniques and enhanced computational power this parameter can be eliminated.

On the other hand side the model is quite successful in describing experimental results.

- 5 - Our model results offer a first time explanation for an observation previously reported by Chatman et al.^{68, 71} which was not discussed in detail at the time. The relatively small increase of measured surface potential with increasing pH within the plateau region is at odds with all the expectations for common oxide-water interface models. Apparently the model designed here for the aged hematite (001) (Figure 9, top panel) is able to cover this behavior. Actually, the increase of surface potential with increasing pH reported by Chatman et al.⁷¹ could be seen as independent support for our model concept.
- 10 - The model also has the potential to describe the experimentally observed offset of the protonation/deprotonation with variable salt content⁶⁷. Usually a surface complexation would treat such experimental observations with one consistent set of parameters (extrapolated to infinite dilution). However, in the cited case it was necessary to apply different pK values for the data measured at the different salt contents.
- 15

20 Conclusions

The present study investigates transient changes at the hematite (001) surface upon aging in aqueous solutions. We observe changes with time in the zeta-potential and the surface diffraction data, while the surface potential response remains unaffected by the structural changes. AFM investigations show that the presence of water and electrolyte solutions affects the surface roughness of our sample. The initially very smooth surface becomes rougher in the presence of water. The surface diffraction data suggest that the fresh surface is not well hydrated. In particular the singly coordinated groups appear neither to affect the pH response nor to influence the zeta-potentials of the fresh surface. A bond-valence analysis of the surface diffraction data supports the lack of hydration in that these aquo-groups are well satisfied in terms of bond valence. With time these reactive groups become more reactive, probably due to a change in bond distances that triggers or is triggered by interactions with water. In the case of the fresh hematite, the adjacent water layer, which is expected to be weakly structured similar as on a hydrophobic surface, dominates the observed zeta-potentials via preferential hydroxide adsorption in that layer. The inner layer becomes affected by protonation (low pH) and deprotonation (high pH) of the doubly coordinated groups, and salt ion adsorption, which allows to explain the measured surface potentials, while the singly coordinated groups remain inactive, similarly to a previous suggestions^{82, 83}.

40 The surface diffraction data for the aged surface show distinct water adsorption. Consequently, the model for the aged surface involves both groups and the action of the singly-coordinated groups allows to explain the high IEP observed. Salt ion adsorption and doubly coordinated surface groups account for the surface potential response, which remains unchanged upon aging. The parameters used in the models are in the range expected based on previous investigations on related systems.

45

Acknowledgements

CTR measurements are performed at GeoSoilEnviroCARS (Sector 13), Advanced Photon Source (APS), Argonne National Laboratory. GeoSoilEnviroCARS is supported by the National Science Foundation - Earth Sciences (EAR-1128799) and Department of Energy- GeoSciences (DE-FG02-94ER14466). This research used resources of the Advanced Photon Source, a U.S. Department of Energy (DOE) Office of Science User Facility operated for the DOE Office of Science by Argonne National Laboratory under Contract No. DE-AC02-06CH11357.

10

Notes and references

^a Institut für Nukleare Entsorgung, Karlsruher Institut für Technologie, P.O. Box 3640, 76021 Karlsruhe, Germany. Fax: 49 721 608 2 3927; Tel: 49 721 608 2 4023; E-mail: Johannes.luetzenkirchen@kit.edu, frank.heberling@kit.edu

^b Laboratory of Physical Chemistry, Department of Chemistry, Faculty of Science, University of Zagreb, Horvatovac 102a, 10001 Zagreb, Croatia. E-mail: nkallay@chem.pmf.hr, tajana@chem.pmf.hr, fsupljika@chem.pmf.hr.

^c Oxford Instruments GmbH, c/o Asylum Research, Hauptstrasse 161, DE-68259 Mannheim, Germany. E-mail: Florian.Johann@oxinst.com, Ludger.Weisser@oxinst.com

^d GeoSoilEnviroCars, University of Chicago, 5640 South Ellis, Chicago, IL 60637, USA. E-mail: eng@cars.uchicago.edu

Electronic Supplementary Information (ESI) available: ESI includes details on the surface diffraction model and surface complexation modelling for both fresh and aged hematite-001. See DOI: 10.1039/b000000x/

1. C. Bataillon, F. Bouchon, C. Chainais-Hillairet, C. Desgranges, E. Hoarau, F. Martin, S. Perrin, M. Tupin and J. Talandier, *Electrochimica Acta*, 2010, **55**, 4451-4467.
2. M. Finšgar and J. Jackson, *Corrosion Science*, 2014, **86**, 17-41.
3. F. F. Eliyan and A. Alfantazi, *Corrosion*, 2014, **70**, 880-898.
4. J. Brunelle, *Pure and Applied Chemistry*, 1978, **50**, 1211-1229.
5. J. A. Schwarz, C. Contescu and A. Contescu, *Chemical Reviews*, 1995, **95**, 477-510.
6. T. Mang, B. Breitscheidel, P. Polanek and H. Knozinger, *Appl. Catal. A-Gen.*, 1993, **106**, 239-258.
7. W. Stumm, *Colloids and Surfaces A: Physicochemical and Engineering Aspects*, 1997, **120**, 143-166.
8. T. Hiemstra, *Langmuir*, 2012, **28**, 15614-15623.
9. Z. Zhang, P. Fenter, L. Cheng, N. C. Sturchio, M. J. Bedzyk, M. Predota, A. Bandura, J. D. Kubicki, S. N. Lvov, P. T. Cummings, A. A. Chialvo, M. K. Ridley, P. Benezeth, L. Anovitz, D. A. Palmer, M. L. Machesky and D. J. Wesolowski, *Langmuir*, 2004, **20**, 4954-4969.
10. G. E. Schaumann, A. Philippe, M. Bundschuh, G. Metreveli, S. Klitzke, D. Rakcheev, A. Grün, S. K. Kumahor, M. Kühn, T. Baumann, F. Lang, W. Manz, R. Schulz and H.-J. Vogel, *Science of The Total Environment*.

11. A. Massarsky, V. L. Trudeau and T. W. Moon, *Environmental Toxicology and Pharmacology*, 2014, **38**, 861-873.
12. S. Wagner, A. Gondikas, E. Neubauer, T. Hofmann and F. von der Kammer, *Angewandte Chemie International Edition*, 2014, **53**, 12398-12419.
- 5 13. J. A. Davis and K. F. Hayes, *Geochemical processes at mineral surfaces*, American Chemical Society Washington, DC, 1986.
14. P. Fenter and N. C. Sturchio, *Progress in Surface Science*, 2004, **77**, 171-258.
15. A. F. White and S. L. Brantley, *Chemical Weathering Rates of Silicate Minerals*, 1995, **31**, 1-22.
- 10 16. J. Bachmann and R. R. van der Ploeg, *Journal of Plant Nutrition and Soil Science*, 2002, **165**, 468.
17. H. B. Bradl, *Journal of Colloid and Interface Science*, 2004, **277**, 1-18.
18. G. Sposito, *The chemistry of soils*, Oxford university press, 2008.
19. C. E. Weaver and L. D. Pollard, *The chemistry of clay minerals*, Elsevier, 2011.
- 15 20. S. L. Swartzen-Allen and E. Matijevic, *Chemical Reviews*, 1974, **74**, 385-400.
21. G. Lagaly and S. Ziesmer, *Advances in Colloid and Interface Science*, 2003, **100**, 105-128.
22. J. Tolls, *Environmental Science & Technology*, 2001, **35**, 3397-3406.
23. W. Stumm and J. J. Morgan, *Aquatic chemistry: chemical equilibria and rates in natural waters*, John Wiley & Sons, 2012.
- 20 24. R. P. Schwarzenbach, P. M. Gschwend and D. M. Imboden, *Environmental organic chemistry*, John Wiley & Sons, 2005.
25. Y. Wang, *Chemical Geology*, 2014, **378-379**, 1-23.
26. D. Langmuir, P. Hall and J. Drever, *Environmental Geochemistry*, Prentice Hall, New Jersey, 1997.
- 25 27. Z. Navrátilová and P. Kula, *Electroanalysis*, 2003, **15**, 837-846.
28. L. Charlet and A. Manceau, *Int. J. Environ. Anal. Chem.*, 1992, **46**, 97-108.
29. J. G. Catalano, *Geochim. Cosmochim. Acta*, 2011, **75**, 2062-2071.
30. L. Zhang, C. Tian, G. A. Waychunas and Y. R. Shen, *J. Am. Chem. Soc.*, 2008, **130**, 7686-7694.
31. M. Sulpizi, M. Salanne, M. Sprik and M. P. Gaigeot, *J. Phys. Chem. Lett.*, 2013, **4**, 83-87.
- 30 32. J. Luetzenkirchen, R. Zimmermann, T. Preocanin, A. Filby, T. Kupcik, D. Kuettner, A. Abdelmonem, D. Schild, T. Rabung, M. Plaschke, F. Brandenstein, C. Werner and H. Geckeis, *Advances in Colloid and Interface Science*, 2010, **157**, 61-74.
33. J. K. Beattie, A. M. Djerdjev, A. Gray-Weale, N. Kallay, J. Luetzenkirchen, T. Preocanin and A. Selmani, *Journal of Colloid and Interface Science*, 2014, **422**, 54-57.
- 35 34. P. Creux, J. Lachaise, A. Graciaa, J. K. Beattie and A. M. Djerdjev, *Journal of Physical Chemistry B*, 2009, **113**, 14146-14150.
35. R. Zimmermann, N. Rein and C. Werner, *Physical Chemistry Chemical Physics*, 2009, **11**, 4360-4364.
36. M. Corti, M. Bonomo and A. Raudino, *Langmuir*, 2012, **28**, 6060-6066.
- 40 37. V. Kuznetsov and G. Papastavrou, *Journal of Physical Chemistry C*, 2014, **118**, 2673-2685.
38. T. Cecchi, *Journal of Physical Chemistry C*, 2013, **117**, 25579-25585.
39. P. Jungwirth, *Faraday Discuss.*, 2009, **141**, 9-30.
40. V. L. Shapovalov, H. Mohwald, O. V. Konovalov and V. Knecht, *Physical Chemistry Chemical Physics*, 2013, **15**, 13991-13998.
- 45 41. B. Winter, M. Faubel, R. Vacha and P. Jungwirth, *Chemical Physics Letters*, 2009, **474**, 241-247.

42. J.-S. Samson, R. Scheu, N. Smolentsev, S. W. Rick and S. Roke, *Chemical Physics Letters*, 2014, **615**, 124-131.
43. J. Luetzenkirchen, T. Preocanin and N. Kallay, *Physical Chemistry Chemical Physics*, 2008, **10**, 4946-4955.
- 5 44. R. Zimmermann, U. Freudenberg, R. Schweiss, D. Kuettner and C. Werner, *Current Opinion in Colloid & Interface Science*, 2010, **15**, 196-202.
45. T. W. Healy and D. W. Fuerstenau, *Journal of Colloid and Interface Science*, 2007, **309**, 183-188.
46. N. Kallay and D. Cakara, *Journal of Colloid and Interface Science*, 2000, **232**, 81-85.
- 10 47. N. Kallay, A. Cop, E. Chibowski and L. Holysz, *Journal of Colloid and Interface Science*, 2003, **259**, 89-96.
48. M. Takahashi, *Journal of Physical Chemistry B*, 2005, **109**, 21858-21864.
49. T. Hiemstra, J. C. M. Dewit and W. H. Vanriemsdijk, *Journal of Colloid and Interface Science*, 1989, **133**, 105-117.
- 15 50. T. Hiemstra, W. H. Vanriemsdijk and G. H. Bolt, *Journal of Colloid and Interface Science*, 1989, **133**, 91-104.
51. T. Hiemstra, P. Venema and W. H. VanRiemsdijk, *Journal of Colloid and Interface Science*, 1996, **184**, 680-692.
52. P. Venema, T. Hiemstra, P. G. Weidler and W. H. van Riemsdijk, *Journal of Colloid and Interface Science*, 1998, **198**, 282-295.
- 20 53. J. P. Fitts, X. M. Shang, G. W. Flynn, T. F. Heinz and K. B. Eisenthal, *Journal of Physical Chemistry B*, 2005, **109**, 7981-7986.
54. T. Hiemstra and W. H. Van Riemsdijk, *Langmuir*, 1999, **15**, 8045-8051.
55. D. Yang, M. Krasowska, R. Sedev and J. Ralston, *Physical Chemistry Chemical Physics*, 2010, **12**, 13724-13729.
- 25 56. N. Kallay, T. Preocanin, F. Supljika, J. Luetzenkirchen and M. Lovkovic, *Journal of Colloid and Interface Science*, 2012, **375**, 167-171.
57. A. Selmani, J. Luetzenkirchen, N. Kallay and T. Preocanin, *Journal of Physics-Condensed Matter*, 2014, **26**.
- 30 58. R. Vacha, R. Zangi, J. Engberts and P. Jungwirth, *Journal of Physical Chemistry C*, 2008, **112**, 7689-7692.
59. J. Luetzenkirchen, *Langmuir*, 2013, **29**, 7726-7734.
60. A. G. Stack, S. R. Higgins and C. M. Eggleston, *Geochim. Cosmochim. Acta*, 2001, **65**, 3055-3063.
- 35 61. K. S. Tanwar, S. C. Petitto, S. K. Ghose, P. J. Eng and T. P. Trainor, *Geochim. Cosmochim. Acta*, 2009, **73**, 4346-4365.
62. T. P. Trainor, A. M. Chaka, P. J. Eng, M. Newville, G. A. Waychunas, J. G. Catalano and G. E. Brown, *Surface Science*, 2004, **573**, 204-224.
63. X. G. Wang, W. Weiss, S. K. Shaikhutdinov, M. Ritter, M. Petersen, F. Wagner, R. Schlogl and M. Scheffler, *Phys. Rev. Lett.*, 1998, **81**, 1038-1041.
- 40 64. C. M. Eggleston, A. G. Stack, K. M. Rosso, S. R. Higgins, A. M. Bice, S. W. Boese, R. D. Pribyl and J. J. Nichols, *Geochim. Cosmochim. Acta*, 2003, **67**, 985-1000.
65. C. M. Eggleston, A. G. Stack, K. M. Rosso and A. M. Bice, *Geochem. Trans.*, 2004, **5**, 33-40.
66. P. Liu, T. Kendelewicz, G. E. Brown Jr, E. J. Nelson and S. A. Chambers, *Surface Science*, **417**, 53-65.
- 45 67. J.-F. Boily, S. Chatman and K. M. Rosso, *Geochim. Cosmochim. Acta*, 2011, **75**, 4113-4124.

68. S. Chatman, P. Zarzycki and K. M. Rosso, *Physical Chemistry Chemical Physics*, 2013, **15**, 13911-13921.
69. N. Kallay and T. Preocanin, *Journal of Colloid and Interface Science*, 2008, **318**, 290-295.
70. J. Luetzenkirchen, T. Preocanin, F. Stipic, F. Heberling, J. Rosenqvist and N. Kallay, *Geochim. Cosmochim. Acta*, 2013, **120**, 479-486.
71. S. Chatman, P. Zarzycki, T. Preocanin and K. M. Rosso, *Journal of Colloid and Interface Science*, 2013, **391**, 125-134.
72. M. M. Gentleman and J. A. Ruud, *Langmuir*, 2010, **26**, 1408-1411.
73. E. Anim-Danso, Y. Zhang and A. Dhinojwala, *J. Am. Chem. Soc.*, 2013, **135**, 8496-8499.
74. B. M. Cabanas, J. Luetzenkirchen, S. Leclercq, P. Barboux and G. Lefevre, *Journal of Nuclear Materials*, 2012, **430**, 150-155.
75. S. A. de Vries, P. Goedtkindt, W. J. Huisman, M. J. Zwanenburg, R. Feidenhans'l, S. L. Bennett, D. M. Smilgies, A. Stierle, J. J. De Yoreo, W. J. P. van Enkevort, P. Bennema and E. Vlieg, *J. Cryst. Growth*, 1999, **205**, 202-214.
76. I. D. Brown and D. Altermatt, *Acta Crystallographica Section B-Structural Science*, 1985, **41**, 244-247.
77. R. Zimmermann, S. Dukhin and C. Werner, *Journal of Physical Chemistry B*, 2001, **105**, 8544-8549.
78. G. V. Franks and Y. Gan, *Journal of the American Ceramic Society*, 2007, **90**, 3373-3388.
79. S. Roessler, R. Zimmermann, D. Scharnweber, C. Werner and H. Worch, *Colloids and Surfaces B: Biointerfaces*, 2002, **26**, 387-395.
80. D. Rothenstein, B. Claasen, B. Omiecinski, P. Lammel and J. Bill, *J. Am. Chem. Soc.*, 2012, **134**, 12547-12556.
81. A. Kiejna and T. Pabisiak, *The Journal of Physical Chemistry C*, 2013, **117**, 24339-24344.
82. I. Siretanu, D. Ebeling, M. P. Andersson, S. L. S. Stipp, A. Philipse, M. C. Stuart, D. van den Ende and F. Mugele, *Scientific Reports*, 2014, **4**.
83. A. Shchukarev, J.-F. Boily and A. R. Felmy, *Journal of Physical Chemistry C*, 2007, **111**, 18307-18316.
84. J. Rosenqvist, P. Persson and S. Sjöberg, *Langmuir*, 2002, **18**, 4598-4604.
85. A. Shchukarev and S. Sjöberg, *Surface Science*, 2005, **584**, 106-112.
86. F. Takeshi, *Science and Technology of Advanced Materials*, 2010, **11**, 033003.
87. M. Kosmulski, *Chemical Properties of Material Surfaces*, CRC Press, 2001.
88. J. Luetzenkirchen, A. Abdelmonem, R. Weerasooriya, F. Heberling, V. Metz and R. Marsac, *Geochem. Trans.*, 2014, **15**.
89. E. Maczka, J. Luetzenkirchen and M. Kosmulski, *Journal of Colloid and Interface Science*, 2013, **393**, 228-233.